*Progress In Electromagnetics Research B, Vol. 53, 399–415, 2013*

# GENERALIZED IMPEDANCE-TRANSFORMING DUAL-BAND BRANCH-LINE COUPLERS FOR ARBITRARY COUPLING LEVELS

**Qiang Liu[1, 2, *], Yuanan Liu[1], Yongle Wu[1, 3], Junyu Shen[1], Shulan Li[1], Cuiping Yu[1], and Ming Su[1]**

[1]School of Electronic Engineering, Beijing University of Posts and Telecommunications, Beijing 100876, China

[2]School of Physics and Electronic Science, Hunan University of Science and Technology, Xiangtan 411201, China

[3]State Key Laboratory of Millimeter Waves, Southeast University, Nanjing 210096, China

**Abstract**—High-performance dual-band Doherty power amplifier and non-uniform circularly polarized antenna array require impedance-transforming unequal dual-band 90° branch-line couplers for power dividing and phase shifting in the feed networks. In this paper, an analytical design methodology of generalized impedance-transforming dual-band branch-line couplers for arbitrary coupling levels is proposed. The coupler features wide range of realizable frequency ratio, multiple flexible selections of open- or short-circuited and pi- or T-network topologies. For demonstration, four numerical examples with different parameters are presented. Furthermore, two microstrip couplers based on open-circuited pi- and T-network topologies were fabricated and measured. The measured results show good performance at dual 1.8/3.45 GHz bands. The fractional bandwidths defined by the fluctuation of the coupling level and the phase difference less than ±0.5 dB and ±5° are up to 17% and 18%, 18% and 2% for open-circuited pi- and T-network topologies, respectively.

*Received 17 June 2013, Accepted 10 August 2013, Scheduled 21 August 2013*

* Corresponding author: Qiang Liu (lqxx1982@gmail.com).

## 1. INTRODUCTION

Branch-line coupler is one of the most essential passive components for RF and microwave circuits and systems, and it is applied to the design of various amplifiers, antenna arrays, mixers, etc. The original branch-line coupler [1] operates only at single band and suffers from disadvantages of narrow bandwidth. In the past decades, there have been many literatures about several new properties of branch-line coupler for miniaturizing the circuit sizes and cutting down the cost, such as dual- or multi-band operations [2–8], arbitrary coupling levels [9, 10], inherent transforming [11, 12], arbitrary output phase difference [13, 14], and co-design with filter [15, 16]. For the dual-band branch-line couplers, approaches based on the introduction of the suitable stub lines in a standard branch-line coupler structure [2–4], adopting composite right/left-handed transmission line structures [5], and inserting a transmission line section at the input ports [6] have been proposed. Tri- and quad-band branch-line couplers with controllable operating frequencies were reported [7, 8]. With respect to arbitrary coupling levels, branch-line couplers integrating quarter-wave transformers at each port for bandwidth enhancement and employing the stepped-impedance section with open stubs at two ends for dual-band operation were proposed [9, 10]. In addition, for removing additional impedance transformer and decreasing circuit size and cost, asymmetric branch-line couplers terminated by arbitrary impedances were reported in [11, 12], and arbitrary phase-difference coupler was presented in [13, 14]. Furthermore, with using the open-ended coupled lines instead of branch lines and port feeding lines, filter-couplers were proposed in literatures [15, 16], respectively.

With the rapid development of modern wireless communication systems, dual-band Doherty power amplifier [17] and dual-band- or dual-circularly polarized antenna and antenna array [18–20] featured lower cost and compact size have drawn much attention recently. Therefore, the branch-line couplers as the key components of it and several functions are required simultaneously, such as dual-band operation, arbitrary coupling levels, and inherent impedance transforming. Unfortunately, there is a ***vacuum*** in the field of this kind of branch-line coupler.

In this paper, a novel design of a dual-band planar asymmetric branch-line coupler terminated by arbitrary impedances for arbitrary coupling levels is proposed. The coupler features wide range of realizable frequency ratio, multiple flexible selections of open- or short-circuited and pi- or T-network topologies. Section 2 presents circuit structure and analytical design theory of dual-band asymmetric

coupler. The two different kinds of dual-band pi- and T-networks for substituting the branch-lines of the asymmetric coupler are analyzed in Section 3. For demonstration purpose, four numerical examples with different parameters are presented in Section 4. At last, two dual-band asymmetric microstrip couplers based on open-circuited pi- and T-network topologies were fabricated and measured in Section 5, and electromagnetic (EM) simulation and experimental results are demonstrated to validate the analytical design methodology of the dual-band planar asymmetric branch-line couplers terminated by arbitrary impedances for arbitrary coupling levels.

## 2. CIRCUIT STRUCTURE AND DESIGN THEORY OF DUAL-BAND ASYMMETRIC COUPLER

The schematic diagram of the proposed dual-band planar asymmetric branch-line coupler terminated by arbitrary real impedances for arbitrary coupling levels is illustrated in Fig. 1. The whole structure of the proposed coupler is asymmetric and terminated by four different port impedances $R_i$ ($i = 1, 2, 3, 4$). For achieving dual-band operation, the four different dual-band branch lines with different characteristic impedances are $Z_{Ci}$ ($i = 1, 2, 3, 4$) instead of the conventional single-band $\lambda/4$ impedance transformer, and the equivalent electrical lengths are $\pm\pi/2$ at the two desired frequencies, $f_1$ and $f_2$, respectively. The value of the frequency ratio $k = f_2/f_1$ is decided according to the required dual band specification.

The proposed dual-band asymmetric branch-line coupler is reciprocal due to its passive property. Moreover, the coupler is

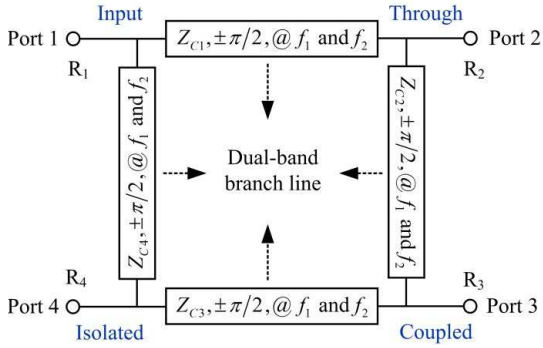


**Figure 1.** Schematic of the proposed dual-band asymmetric branch-line coupler.

assumed to be lossless for facilitating the network analysis. Under the rigorous constraint conditions, including the coupling coefficient $C$, the quadrature phase difference $\pm\pi/2$, the ideal matching $S_{11} = 0$, and the perfect isolation $S_{41} = 0$, the scattering matrix $[S]$ of the proposed coupler shown in Fig. 1 can be defined by

$$\begin{bmatrix} a_1 \\ a_2 \\ a_3 \\ a_4 \end{bmatrix} = \begin{bmatrix} S_{11} & S_{12} & S_{13} & S_{14} \\ S_{21} & S_{22} & S_{23} & S_{24} \\ S_{31} & S_{32} & S_{33} & S_{34} \\ S_{41} & S_{42} & S_{43} & S_{44} \end{bmatrix} \begin{bmatrix} b_1 \\ b_2 \\ b_3 \\ b_4 \end{bmatrix} = \begin{bmatrix} 0 & S_{12} & S_{13} & 0 \\ S_{21} & 0 & 0 & S_{24} \\ S_{31} & 0 & 0 & S_{34} \\ 0 & S_{42} & S_{43} & 0 \end{bmatrix} \begin{bmatrix} b_1 \\ b_2 \\ b_3 \\ b_4 \end{bmatrix} \quad (1a)$$

$$S_{12} = S_{21} = S_{34} = S_{43} = \pm\alpha \quad (1b)$$

$$S_{13} = S_{31} = S_{24} = S_{42} = \pm j\beta \quad (1c)$$

$$\alpha^2 + \beta^2 = 1 \quad (1d)$$

$$C = -20 \lg \beta (\mathrm{dB}) \quad (1e)$$

$$T = -20 \lg \alpha (\mathrm{dB}) \quad (1f)$$

where $a_i$ and $b_i$ are the incident and reflected normalized wave at port $i$ ($i = 1, 2, 3, 4$); $T$ is the through coefficient; $\alpha$ and $\beta$ are the wave amplitude at through and coupled ports, respectively.

As there is no symmetric plane in the structure, the dual-band asymmetric branch-line coupler in Fig. 1 cannot be solved by conventional methods of even- and odd-mode analysis [21]. Therefore, the simplified circuit design method in [22] is employed to analyze this coupler. Herein, assuming port 4 terminated in a reflection coefficient $\Gamma_4$ in Fig. 1, by a straightforward manipulation, the relationship between the incident and reflected voltage waves based on the scattering parameters can be rewritten as

$$\begin{bmatrix} b_1 \\ b_2 \\ b_3 \end{bmatrix} = \begin{bmatrix} S_{11} & S_{12} & S_{13} \\ S_{21} & S_{22} & S_{23} \\ S_{31} & S_{32} & S_{33} \end{bmatrix} \begin{bmatrix} a_1 \\ 0 \\ 0 \end{bmatrix} + \frac{S_{41} a_1 \Gamma_4}{1 - \Gamma_4 S_{44}} \begin{bmatrix} S_{14} \\ S_{24} \\ S_{34} \end{bmatrix} \quad (2)$$

where $a_1$ is the incident normalized wave at port 1 and $b_i$ the reflected normalized waves at port $i$ ($i = 1, 2, 3$). The perfect isolation $S_{41} = 0$ in (2) indicates that there is only power split between ports 2 and 3, and no correlation with $\Gamma_4$ in terms of port 1 excitation. Therefore, the asymmetric branch-line coupler can be simplified to an equivalent circuit as shown in Fig. 2.

Due to the connected line structure, the mechanism of the coupler can be explained as an ohmic connection. The normalized total power "1" coming from port 1 is split into two ways after going through point A, as shown in Fig. 2. Based on the node voltage equations at point A and considering the power split ratio of the output power on resistances $R_2$ at port 2 and $R_3$ at port 3 equal to $P = \alpha^2/\beta^2$, the all

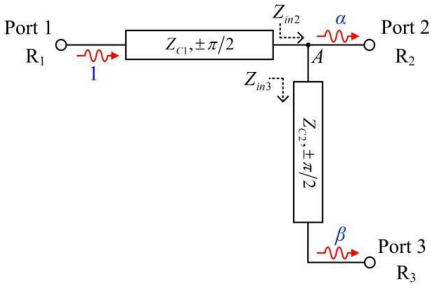


**Figure 2.** Equivalent circuit of the coupler as excited at port 1 for $S_{41} = 0$.

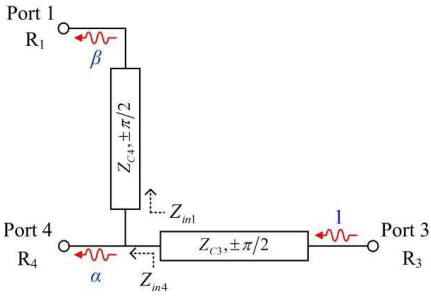


**Figure 3.** The removed circuit of the coupler for the isolation condition $S_{41} = 0$.

resistance relationships in Fig. 2 can be obtained

$$Z_{in3} = \left(\frac{\alpha^2}{\beta^2}\right) R_2 \tag{3}$$

$$Z_{in2} = \frac{Z_{in3} R_2}{Z_{in3} + R_2} = \alpha^2 R_2 \tag{4}$$

the relationship of (1d) is used for simplification. For satisfying the isolation condition $S_{41} = 0$, the part of the circuit shown in Fig. 3 is removed from Fig. 2. Due to reciprocity, the circuit can be considered as being excited at port 3, and the resistance relationships are derived similarly as

$$Z_{in1} = \left(\frac{\alpha^2}{\beta^2}\right) R_4 \tag{5}$$

$$Z_{in4} = \frac{Z_{in1} R_4}{Z_{in1} + R_4} = \alpha^2 R_4 \tag{6}$$

Based on (3) to (6), one can compute the desirable characteristic impedances $Z_{Ci}$ ($i = 1, 2, 3, 4$) of the four dual-band branch lines in Fig. 1 as follows

$$Z_{C1} = \sqrt{R_1 Z_{in2}} = \alpha \sqrt{R_1 R_2} \tag{7a}$$

$$Z_{C2} = \sqrt{Z_{in3} R_3} = \frac{\alpha}{\beta} \sqrt{R_2 R_3} \tag{7b}$$

$$Z_{C3} = \sqrt{R_3 Z_{in4}} = \alpha \sqrt{R_3 R_4} \tag{7c}$$

$$Z_{C4} = \sqrt{Z_{in1} R_1} = \frac{\alpha}{\beta} \sqrt{R_1 R_4} \tag{7d}$$

In addition, the equivalent electrical lengths of the dual-band branch line should be equal $\pm\pi/2$ at the two desired operating

frequencies, $f_1$ and $f_2$, respectively. Therefore, the next task is to design the circuit structures and parameters of these networks for the dual-band branch lines.

## 3. ANALYSIS OF NETWORKS FOR DUAL-BAND BRANCH-LINES

### 3.1. Analysis of Pi-network

Figure 4 shows the desired dual-band branch-line with characteristic impedances $Z_C$ and its one of the implementing pi-network circuit structures, which is composed of a section of transmission line ($Z_{PA}$, $\theta_{PA}$) and a pair of shunt reactive elements ($jY_P$). Due to reciprocal property, the $ABCD$-matrix of the pi-network shown in Fig. 4(b) can be expressed as

$$\begin{bmatrix} A_P & B_P \\ C_P & D_P \end{bmatrix} = \begin{bmatrix} 1 & 0 \\ jY_P & 1 \end{bmatrix} \begin{bmatrix} \cos\theta_{PA} & jZ_{PA}\sin\theta_{PA} \\ j\sin\theta_{PA}/Z_{PA} & \cos\theta_{PA} \end{bmatrix} \begin{bmatrix} 1 & 0 \\ jY_P & 1 \end{bmatrix} \quad (8)$$

where the elements of $ABCD$-matrix are given by

$$A_P = D_P = \cos\theta_{PA} - Z_{PA}Y_P\sin\theta_{PA} \quad (9a)$$

$$B_P = jZ_{PA}\sin\theta_{PA} \quad (9b)$$

$$C_P = jY_P\sin\theta_{PA}\left(1 - Z_{PA}^2Y_P^2 + 2Z_{PA}Y_P\cot\theta_{PA}\right) \quad (9c)$$

Since the pi-network is intended to substitute the desired dual-band branch-line, the $ABCD$-matrixes of pi-network and the desired dual-band branch-line should be equivalent and can be written as

$$\begin{bmatrix} A_P & B_P \\ C_P & D_P \end{bmatrix} = \begin{bmatrix} 0 & \pm jZ_C \\ \pm j/Z_C & 0 \end{bmatrix} \quad (10)$$

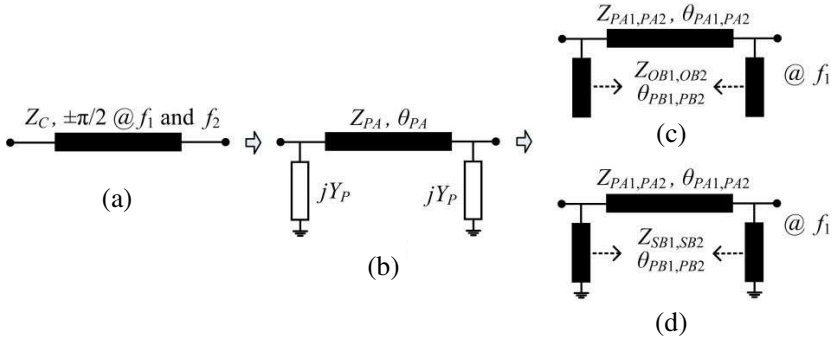


**Figure 4.** The desired dual-band branch-line and its implementing pi-network circuit structure.

For the purpose of dual-band operation, the parameters of the pi-network can be derived by solving (10) as follows

$$Z_{PA1,PA2} = \frac{Z_C}{\sin\theta_{PA1,PA2}} \tag{11a}$$

$$Y_{P1,P2} = \frac{\cos\theta_{PA1,PA2}}{Z_C} \tag{11b}$$

$$\begin{aligned} \theta_{PA1} &= \frac{n\pi}{(k+1)} \ @\ f_1 \\ \theta_{PA2} &= \frac{n\pi}{(k-1)} \ @\ f_1 \end{aligned} \tag{11c}$$

where $k = f_2/f_1$ is the frequency ratio and $n = 1, 2, 3, \ldots$, $Z_{PA1}$, $Z_{PA2}$ and $\theta_{PA1}$, $\theta_{PA2}$ are the characteristic impedances and the electrical lengths at frequency $f_1$ for the two cases of '+' and '−' in (10), respectively. The shunt reactive elements ($jY_{P1}$ and $jY_{P2}$) can be realized by two different circuit structures as shown in Fig. 4(c) and Fig. 4(d), which are open- and short-circuited stubs. For the provision of more degrees of design freedom, the two circuit structures are considered as follows

$$Z_{OB1,OB2} = \frac{Z_C}{\cos\theta_{PA1,PA2}} \tan\theta_{PB1,PB2} \text{ for open-circuit stub} \tag{12a}$$

$$Z_{SB1,SB2} = \frac{Z_C}{\cos\theta_{PA1,PA2}} \cot\theta_{PB1,PB2} \text{ for short-circuit stub} \tag{12b}$$

$$\begin{aligned} \theta_{PB1} &= \tfrac{m\pi}{(k+1)} \ @\ f_1 \\ \theta_{PB2} &= \tfrac{m\pi}{(k-1)} \ @\ f_1 \end{aligned} \tag{12c}$$

where $m = 1, 2, 3, \ldots$, $Z_{OB1}$, $Z_{OB2}$, $Z_{SB1}$, $Z_{SB2}$ are the characteristic impedances, and $\theta_{PB1}$, $\theta_{PB2}$ are the electrical lengths at frequency $f_1$ of the open- and short-circuited stubs for the two cases of '+' and '−' in (10), respectively. Seen from (11) and (12), there exist multiple solutions, including the choices of $n$, $m$, open- or short-circuited stubs in (12), and '+' or '−' in (10). However, microwave printed circuit board (PCB) technology limitation, reasonable characteristic impedance between 20 and 120 Ω for microstrip lines, and size reduction put restriction on the choice of the solutions.

It should be mentioned that the range of realizable impedance for the open- and short-circuited stubs of pi-network can be modified to the range of 40 to 240 Ω, since the two paralleled shunt stubs of two different dual-band branch lines in the coupler can be merged into a shunt stub for simplification. For illustration, setting the characteristic impedances $Z_C = 50\,\Omega$, Figs. 5 and 6 give the normalized impedances of the pi-network as functions of the frequency ratio $k$ for open- and

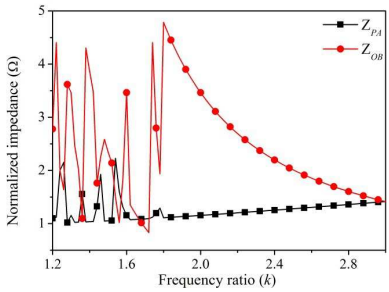


**Figure 5.** Normalized impedances of the open-circuited pi-network versus frequency ratio.

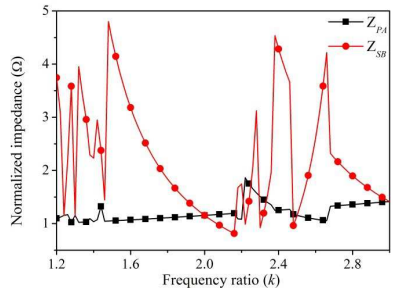


**Figure 6.** Normalized impedances of the short-circuited pi-network versus frequency ratio.

short-circuited topologies. It is found that the frequency ratios from 1.2 to 3 can be realized by a proper choice of $n$ and $m$ in (11) and (12), where $n$ and $m$ are confined to the ranges of 1 to 3 and 1 to 5, respectively.

### 3.2. Analysis of T-network

Figure 7 presents the desired dual-band branch-line and another one of implementing T-network circuit structures, composed by two identical sections of a transmission line ($Z_{TA}$, $\theta_{TA}$) and a shunt reactive elements ($jY_T$). $ABCD$-matrix of the T-network shown in Fig. 7(b) can be expressed as

$$\begin{bmatrix} A_T & B_T \\ C_T & D_T \end{bmatrix} = \begin{bmatrix} \cos\theta_{TA} & jZ_{TA}\sin\theta_{TA} \\ \frac{j\sin\theta_{TA}}{Z_{TA}} & \cos\theta_{TA} \end{bmatrix} \begin{bmatrix} 1 & 0 \\ jY_T & 1 \end{bmatrix} \begin{bmatrix} \cos\theta_{TA} & jZ_{TA}\sin\theta_{TA} \\ \frac{j\sin\theta_{TA}}{Z_{TA}} & \cos\theta_{TA} \end{bmatrix} \tag{13}$$

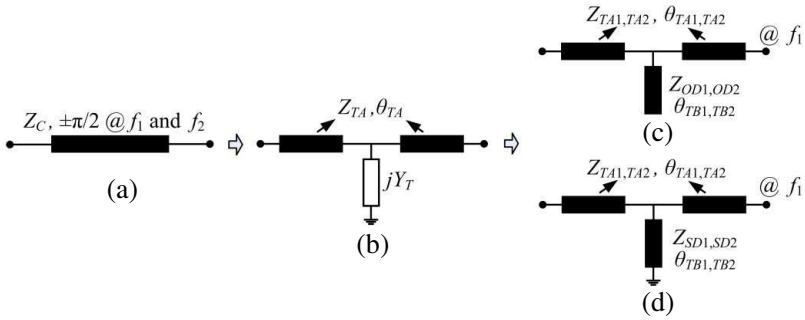


**Figure 7.** The desired dual-band branch-line and its implementing T-network circuit structure.

Since the T-network also substitutes the desired dual-band branch-line, by the same analytical method as in Section 3, the circuit parameters can be derived as follows

$$\begin{bmatrix} A_T & B_T \\ C_T & D_T \end{bmatrix} = \begin{bmatrix} 0 & \pm jZ_C \\ \pm j/Z_C & 0 \end{bmatrix} \tag{14a}$$

$$Z_{TA1,TA2} = \frac{Z_C}{\tan\theta_{TA1,TA2}} \tag{14b}$$

$$Y_{TA1,TA2} = \frac{1-(\tan\theta_{TA1,TA2})^2}{Z_C} \tag{14c}$$

$$Z_{OD1,OD2} = \frac{Z_C \tan\theta_{TB1,TB2}}{1-(\tan\theta_{TA1,TA2})^2} \text{ for open-circuit stub} \tag{14d}$$

$$Z_{SD1,SD2} = \frac{Z_C \cot\theta_{TB1,TB2}}{(\tan\theta_{TA1,TA2})^2-1} \text{ for short-circuit stub} \tag{14e}$$

$$\begin{aligned} \theta_{TA1} &= \tfrac{l\pi}{(k+1)} \ @ \ f_1 \\ \theta_{TA2} &= \tfrac{l\pi}{(k-1)} \ @ \ f_1 \end{aligned} \tag{14f}$$

$$\begin{aligned} \theta_{TB1} &= \tfrac{q\pi}{(k+1)} \ @ \ f_1 \\ \theta_{TB2} &= \tfrac{q\pi}{(k-1)} \ @ \ f_1 \end{aligned} \tag{14g}$$

where $k = f_2/f_1$ is the frequency ratio, and $l$, $q = 1, 2, 3, \ldots$. $Z_{TA1}$, $Z_{TA2}$, $Z_{OD1}$, $Z_{OD2}$, $Z_{SD1}$, $Z_{SD2}$ are the characteristic impedances, and $\theta_{TA1}$. $\theta_{TA2}$, $\theta_{TB1}$, $\theta_{TB2}$ are electrical lengths at frequency $f_1$ of the transmission lines and open- or short-circuited stubs for the two conditions of '+' and '−' in (14a), respectively. Similarly, setting the characteristic impedances $Z_C = 50\,\Omega$, Figs. 8 and 9 give the normalized impedances of the T-network as functions of the frequency ratio $k$ for open- and short-circuited topologies. It should be mentioned that except that the case of $k$ equal to 2 for short-circuited T-network cannot be realized, the frequency ratios $k$ from 1.2 to 2.92 can be achieved by a proper choice of $l$ and $q$ in (14f) and (14g), where the maximum values $l$ and $q$ are equal to 5 and 6, respectively.

## 4. NUMERICAL EXAMPLES OF DUAL-BAND ASYMMETRIC BRANCH-LINE COUPLER

By employing the pi- and T-networks in Section 3 for all four branch-lines shown in Fig. 1, the proposed dual-band asymmetric branch-line coupler terminated by arbitrary real impedances for arbitrary coupling levels is implemented as shown in Fig. 10 and Fig. 11. Herein, the via-less open-circuited topology is adopted to all dual-band branch-lines for fabricating conveniently, and the paralleled shunt stubs of pi-

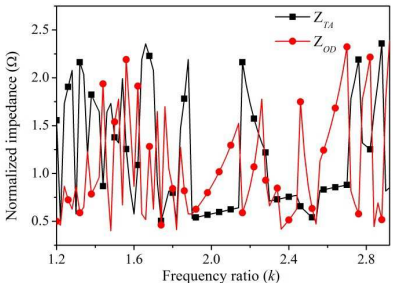


**Figure 8.** Normalized impedances of the open-circuited T-network versus frequency ratio.

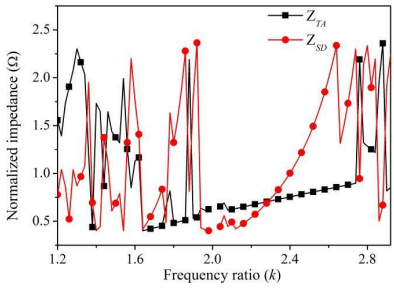


**Figure 9.** Normalized impedances of the short-circuited T-network versus frequency ratio.

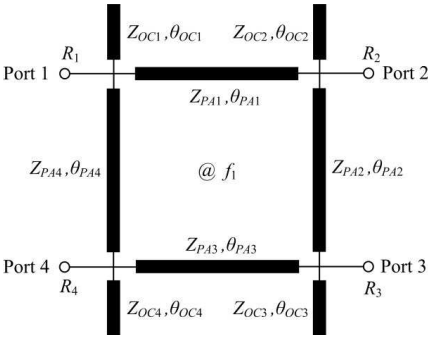


**Figure 10.** The implemented asymmetric branch-line coupler based on open-circuited pi-network.

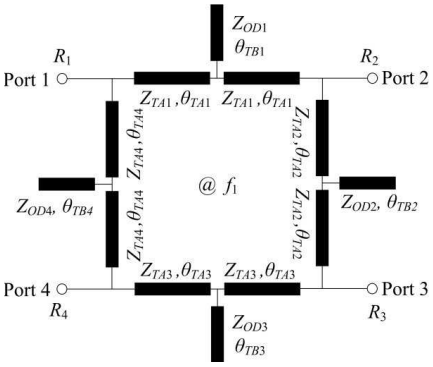


**Figure 11.** The implemented asymmetric branch-line coupler based on open-circuited T-network.

networks are merged for simplification as shown in Fig. 10. Moreover, the electrical lengths of all transmission lines and stubs are presented at the lower operation frequency $f_1$.

In order to verify the proposed analytical design approaches and illustrate the implementation, four numerical examples of typical dual-band asymmetric couplers using pi- and T-network topologies, respectively, are designed and simulated. Here, frequency ratio $k$ equal to 1.92 (for the practical dual 1.8-/3.45-GHz bands of personal communication systems) with coupling level of $C = 4.77$ dB (the power divider ratio equals 3 dB), and frequency ratio $k$ equal to 2.66 (for the practical dual 0.92-/2.45-GHz bands of radio frequency identification

systems) with the coupling level of $C = 6.99\,\text{dB}$ (the power divider ratio equals 6 dB) are chosen as desired objective parameters for the proposed coupler. Moreover, the port impedances of couplers are set arbitrarily. Characteristic impedances of transmission lines and stubs are normalized to the system impedance $Z_0 = 50\,\Omega$ universally, and the first operating frequency $f_1$ of these four examples are normalized to 1 GHz. The detail circuit parameter values of the proposed dual-band asymmetric branch-line couplers are listed in Table 1, which are calculated based on formulas (7), (10)–(14) except that the port impedances are set beforehand arbitrarily.

The scattering parameters ($S$-parameters) and the phase difference between ports 2 (through port) and 3 (coupled port) of the four couplers are presented in Fig. 12. The perfect return loss (RL), isolation, desired coupling level and quadrature phase difference can be achieved at dual bands. As shown in Table 1, the four port

**Table 1.** Circuit parameters values of the couplers.

| **Examples** | **Known parameters** | **Calculated parameters** (@ $f_1$) |
|---|---|---|
| **Coupler A** based on pi-network and open-circuited shunt stubs | $k=1.92$ (1.8/3.45 GHz), $C=4.77$ dB, $T=1.76$ dB, $R_1=0.6$, $R_2=1.2$, $R_3=0.8$, $R_4=1$. | $Z_{PA1}=0.79$, $Z_{PA2}=1.57$, $Z_{PA3}=0.83$, $Z_{PA4}=1.24$, $\theta_{PA}=0.34\pi$. $Z_{OC1}=1.66$, $Z_{OC2}=1.81$, $Z_{OC3}=1.88$, $Z_{OC4}=1.72$, $\theta_{OC}=0.34\pi$. |
| **Coupler B** based on T-network and open-circuited shunt stubs | $k=1.92$ (1.8/3.45 GHz), $C=4.77$ dB, $T=1.76$ dB, $R_1=1.1$, $R_2=1.3$, $R_3=1.5$, $R_4=0.9$. | $Z_{TA1}=0.53$, $Z_{TA2}=1.06$, $Z_{TA3}=0.51$, $Z_{TA4}=0.76$, $\theta_{TA}=0.34\pi$. $Z_{OD1}=0.6$, $Z_{OD2}=1.22$, $Z_{OD3}=0.59$, $Z_{OD4}=0.87$, $\theta_{TB}=0.68\pi$. |
| **Coupler C** based on pi-network and open-circuited shunt stubs | $k=2.66$ (0.92/2.45 GHz), $C=6.99$ dB, $T=0.97$ dB, $R_1=0.9$, $R_2=0.6$, $R_3=1.1$, $R_4=0.8$. | $Z_{PA1}=0.87$, $Z_{PA2}=2.14$, $Z_{PA3}=1.11$, $Z_{PA4}=2.24$, $\theta_{PA}=0.27\pi$. $Z_{OC1}=0.84$, $Z_{OC2}=0.83$, $Z_{OC3}=0.98$, $Z_{OC4}=0.99$, $\theta_{OC}=0.27\pi$. |
| **Coupler D** based on T-network and open-circuited shunt stubs | $k=2.66$ (0.92/2.45 GHz), $C=6.99$ dB, $T=0.97$ dB, $R_1=0.5$, $R_2=0.6$, $R_3=0.6$, $R_4=0.8$. | $Z_{TA1}=0.42$, $Z_{TA2}=1.04$, $Z_{TA3}=0.54$, $Z_{TA4}=1.09$, $\theta_{TA}=0.27\pi$. $Z_{OD1}=0.93$, $Z_{OD2}=2.28$, $Z_{OD3}=1.18$, $Z_{OD4}=2.4$, $\theta_{TB}=0.82\pi$. |

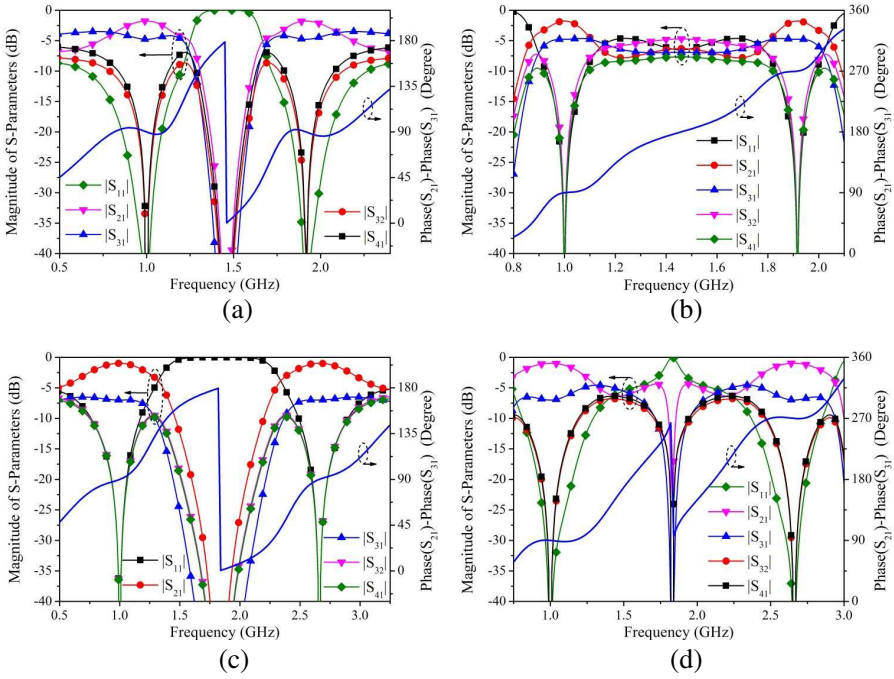


**Figure 12.** The calculated $S$-parameters and phase difference of the couplers, (a) Coupler A, (b) Coupler B, (c) Coupler C, (d) Coupler D.

impedances are different from each other in these four examples, but the ideal performance can also be achieved by using our proposed design approach.

## 5. IMPLEMENTATION AND MEASUREMENT RESULTS

For experimental verification, two dual 1.8-/3.45-GHz bands asymmetric branch-line microstrip couplers with parameter value for the $k$ equal to 1.92, described in Section 4, were modeled and simulated with the aid of the Ansoft HFSS 3-D EM simulator. Considering convenient measurement with 50-Ω ports, four dual-band impedance transformers [23] working at 1.8-/3.45-GHz are added at each port of the couplers. Fig. 13 and Fig. 14 show the simulated EM scattering parameters and the phase differences between ports 2 (through port) and 3 (coupled port). Based on the physical dimensions of the prototype in the Ansoft HFSS simulator, those couplers have been fabricated. The

substrate employed is the Rogers4350B, with a relative permittivity of 3.48, loss tangent of 0.004, and thickness of 0.762 mm. Fig. 15 and Fig. 16 show photographs and dimensions of the dual-band asymmetric microstrip couplers with SMA connectors welded for measurement. $S$-parameter and the phase difference measurements are performed by using the Agilent's four-port network analyzer E5071C over the frequency range from 1.25 to 4 GHz, and the results are shown in Fig. 17 and Fig. 18.

For the coupler based on open-circuited pi-network, seen from Fig. 13, the EM simulated center frequencies are 1.8 and 3.45 GHz. The return losses and isolations are better than 30 and 25 dB. The coupling levels are −5.3 and −4.2 dB. The through coefficients are −1.9

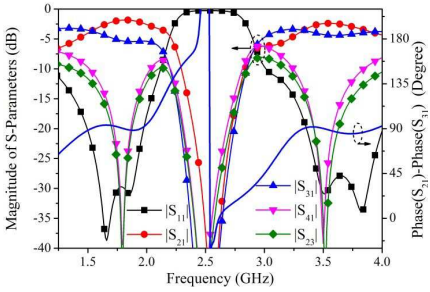


**Figure 13.** The EM simulated $S$-parameters and phase difference of the coupler prototype based on open-circuited pi-network.

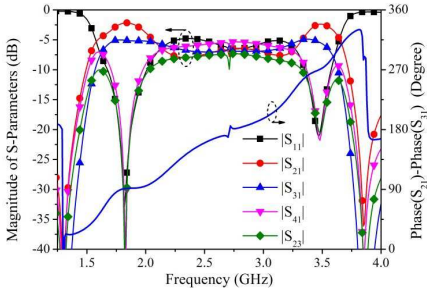


**Figure 14.** The EM simulated $S$-parameters and phase difference of the coupler prototype based on open-circuited T-network.

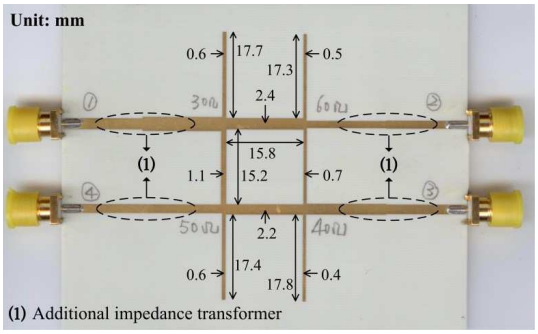


**Figure 15.** Photograph and dimensions of the fabricated coupler based on open-circuited pi-network.

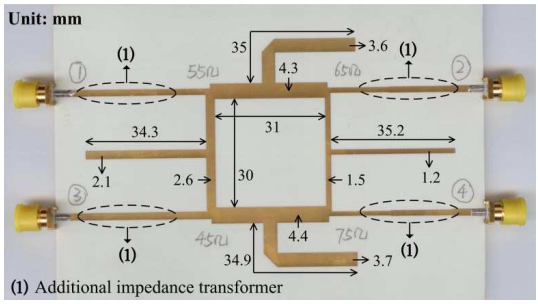


**Figure 16.** Photograph and dimensions of the fabricated coupler based on open-circuited T-network.

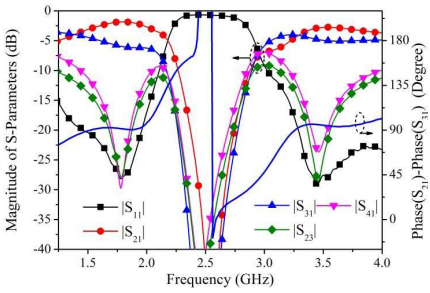


**Figure 17.** The measured *S*-parameters and phase difference of the coupler prototype based on open-circuited pi-network.

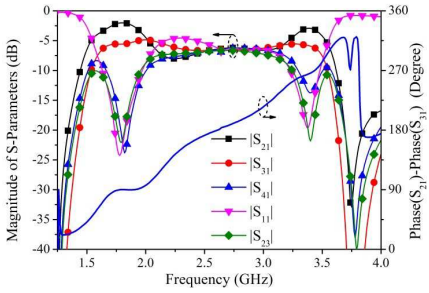


**Figure 18.** The measured *S*-parameters and phase difference of the coupler prototype based on open-circuited T-network.

and −2.6 dB, and the phase differences between through and coupled ports are 90° and 91° at 1.8 and 3.45 GHz, respectively. With the fluctuation of the coupling level and the phase difference less than ±0.5 dB and ±5°, the EM simulated bandwidths of the coupler are over 320 and 350 MHz, with fractional bandwidths of 18% and 10% at 1.8 and 3.45 GHz, respectively. Seen from Fig. 17, the measured center frequencies are 1.8 and 3.45 GHz. The return losses and isolations are better than 27 and 28 dB. The coupling levels are −5.9 and −4.8 dB. The through coefficients are −1.8 and −2.8 dB, and the phase differences between through and coupled ports are 91° and 93° at 1.8 and 3.45 GHz, respectively. With the fluctuation of the coupling level and the phase difference less than ±0.5 dB and ±5°, the measured bandwidths of the coupler are over 300 and 620 MHz, with fractional

bandwidths of 17% and 18% at 1.8 and 3.45 GHz, respectively.

Similarly, for the coupler based on open-circuited T-network, seen from Fig. 14, the EM simulated center frequencies are 1.8 and 3.45 GHz. The return losses and isolations are better than 26 and 19 dB. The coupling levels are $-5$ and $-5.1$ dB. The through coefficients are $-2.3$ and $-2.5$ dB, and the phase differences between through and coupled ports are 89° and 269° at 1.8 and 3.45 GHz, respectively. With the fluctuation of the coupling level and the phase difference less than $\pm 0.5$ dB and $\pm 5°$, the EM simulated bandwidths of the coupler are over 260 and 110 MHz, with fractional bandwidths of 14% and 3% at 1.8 and 3.45 GHz, respectively. Seen from Fig. 18, the measured center frequencies are 1.8 and 3.45 GHz. The return losses and isolations are better than 22 and 13 dB. The coupling levels are $-5.6$ and $-6.4$ dB. The through coefficients are $-2$ and $-3.3$ dB, and the phase differences between through and coupled ports are 90° and 272° at 1.8 and 3.45 GHz, respectively. With the fluctuation of the coupling level and the phase difference less than $\pm 0.5$ dB and $\pm 5°$, the measured bandwidths of the coupler are over 220 and 80 MHz, with fractional bandwidths of 18% and 2% at 1.8 and 3.45 GHz, respectively.

## 6. CONCLUSIONS

An analytical design methodology of a dual-band planar asymmetric branch-line coupler terminated by arbitrary impedances for arbitrary coupling levels is proposed in this paper. The design method is verified by four numerical examples and two typical microstrip experiments. Due to the advantages of arbitrary port impedances and coupling levels, wide range of realizable frequency ratio, multiple flexible selections of open- or short-circuited and pi- or T-network topologies, it can be expected that the coupler is desirable for the design of microwave active circuits and antenna feed networks.

## ACKNOWLEDGMENT

This work was supported in part by the National Natural Science Foundation of China (No. 61001060, No. 61201025, and No. 61201027), the Fundamental Research Funds for the Central Universities (No. 2012RC0301 and No. 2012ZX06), the Open Project of the State Key Laboratory of Millimeter Waves (No. K201316), the Specialized Research Fund for the Doctor Program of Higher Education (No. 20120005120006), and the Fund Project of the Education Department in Hunan Province (No. 11C0517).

## REFERENCES


1. Reed, J. and G. J. Wheeler, "A method of analysis of symmetrical four-port networks," *IEEE Trans. on Microw. Theory and Tech.,* Vol. 4, No. 4, 246–252, Oct. 1956.
2. Cheng, K. K. M. and F. L. Wong, "A novel approach to the design and implementation of dual-band compact planar 90° branch-line coupler," *IEEE Trans. on Microw. Theory and Tech.,* Vol. 52, No. 11, 2458–2463, Nov. 2004.
3. Zhang, H. L. and K. J. Chen, "A stub tapped branch-line coupler for dual-band operations," *IEEE Microw. Wirel. Compon. Lett.,* Vol. 17, No. 2, 106–108, Feb. 2007.
4. Chin, K. S., K. M. Lin, Y. H. Wei, T. H. Tseng, and Y. J. Yang, "Compact dual-band branch-line and rat-race couplers with stepped-impedance-stub lines," *IEEE Trans. on Microw. Theory and Tech.,* Vol. 58, No. 5, 1213–1221, May 2010.
5. Lin, I. H., M. De Vincentis, C. Caloz, and T. Itoh, "Arbitrary dual-band components using composite right/left-handed transmission lines," *IEEE Trans. on Microw. Theory and Tech.,* Vol. 52, No. 4, 1142–1149, Apr. 2004.
6. Kim, H., B. Lee, and M. J. Park, "Dual-band branch-line coupler with port extensions," *IEEE Trans. on Microw. Theory and Tech.,* Vol. 58, No. 3, 651–655, Mar. 2010.
7. Lin, F. and Q. X. Chu, "Tri-band branch-line coupler with T-type and additional port impedance transformers," *2012 IEEE Antennas and Propagation Society International Symposium (APSURSI)*, 8–14, Jul. 2012.
8. Piazzon, L., P. Saad, P. Colantonio, F. Giannini, K. Andersson, and C. Fager, "Branch-line coupler design operating in four arbitrary frequencies," *IEEE Microw. Wirel. Compon. Lett.,* Vol. 22, No. 2, 67–69, Feb. 2012.
9. Lee, S. and Y. Lee, "Wideband branch-line couplers with single-section quarter-wave transformers for arbitrary coupling levels," *IEEE Microw. Wirel. Compon. Lett.,* Vol. 22, No. 1, 19–21, Jan. 2012.
10. Hsu, C. L., J. T. Kuo, and C. W. Chang, "Miniaturized dual-band hybrid couplers with arbitrary power division ratios," *IEEE Trans. on Microw. Theory and Tech.,* Vol. 57, No. 1, 149–156, Jan. 2009.
11. Gupta, R. K., S. E. Anderson, and W. J. Getsinger, "Impedance-transforming 3-dB 90° hybrids," *IEEE Trans. on Microw. Theory and Tech.,* Vol. 35, No. 12, 1303–1307, Dec. 1987.

12. Kumar, S., C. Tannous, and D. Tom, "A multisection broadband impedance transforming branch-line hybrid," *IEEE Trans. on Microw. Theory and Tech.,* Vol. 43, No. 11, 2517–2523, Nov. 1995.
13. Wong, Y. S., S. Y. Zheng, and W. S. Chan, "Quasi-arbitrary phase-difference hybrid coupler," *IEEE Trans. on Microw. Theory and Tech.,* Vol. 60, No. 6, 1530–1539, Jun. 2012.
14. Wu, Y., J. Shen, and Y. Liu, "Comments on 'Quasi-arbitrary phase-difference hybrid coupler'," *IEEE Trans. on Microw. Theory and Tech.,* Vol. 61, No. 4, 1725–1727, Apr. 2013.
15. Wong, Y. S., S. Y. Zheng, and W. S. Chan, "Multifolded bandwidth branch line coupler with filtering characteristic using coupled port feeding," *Progress In Electromagnetics Research*, Vol. 118, 17–35, 2011.
16. Cheng, Y. J., L. Wang, J. Wu, and Y. Fan, "Directional coupler with good restraint outside the passband and its frequency-agile application," *Progress In Electromagnetics Research*, Vol. 135, 759–771, 2013.
17. Rawat, K. and F. M. Ghannouchi, "Design methodology for dual-band doherty power amplifier with performance enhancement using dual-band offset lines," *IEEE Trans. on Industrial Electronics,* Vol. 59, No. 12, 4831–4842, Dec. 2012.
18. Jung, Y. K. and B. Lee, "Dual-band circularly polarized microstrip rfid reader antenna using metamaterial branch-line coupler," *IEEE Trans. Antennas Propag.,* Vol. 60, No. 2, 786–791, Feb. 2012.
19. Garcia-Aguilar, A., J. Inclan-Alonso, L. Vigil-Herrero, J. Fernandez-Gonzalez, and M. Sierra-Perez, "Low-profile dual circularly polarized antenna array for satellite communications in the X band," *IEEE Trans. Antennas Propag.,* Vol. 60, No. 5, 2276–2284, May 2012.
20. Wu, G. L., W. Mu, G. Zhao, and Y. C. Jiao, "A novel design of dual circularly polarized antenna FED by L-strip," *Progress In Electromagnetics Research*, Vol. 79, 39–46, 2008.
21. Ahn, H. R. and B. Kim, "Toward integrated circuit size reduction," *IEEE Microw. Mag.,* Vol. 9, No. 1, 65–75, Feb. 2008.
22. Ahn, H. R. and I. Wolff, "Asymmetric four-port and branch-line hybrids," *IEEE Trans. on Microw. Theory and Tech.*, Vol. 48, No. 9, 1585–1588, Sep. 2000.
23. Monzon, C., "A small dual-frequency transformer in two sections," *IEEE Trans. on Microw. Theory and Tech.,* Vol. 51, No. 4, 1157–1161, Apr. 2003.